Supporting Information

Self-Assembly of a Ginkgo Oligomerization Domain Creates a Sub-10-nm Honeycomb Architecture on Carbon and Silicon Surfaces with Customizable Pores: Implications for Nanoelectronics, Biosensing and Biocatalysis

Elise Jacquier, Pierre-Henri Jouneau, Denis Falconet, Denis Mariolle, Emmanuel Thévenon, Grégory Si Larbi, Raluca Tiron, François Parcy*, Pierre-Henri Elchinger*, Renaud Dumas*

Corresponding Authors

François Parcy - Univ. Grenoble Alpes, CNRS, CEA, INRAE, IRIG-DBSCI-LPCV, 38000 Grenoble, France. Email: francois.parcy@cea.fr

Pierre-Henri Elchinger - Univ. Grenoble Alpes, CEA, CNRS, IRIG-DIESE-SYMMES, 38000 Grenoble, France. Email: pierre-henri.elchinger@cea.fr

Renaud Dumas - Univ. Grenoble Alpes, CNRS, CEA, INRAE, IRIG-DBSCI-LPCV, 38000 Grenoble, France. Email: renaud.dumas@cea.fr

Table S1. Overview on Protein self-assemblies.

Nature of pattern	Self-assembly mechanism	2D Dimension	Lattice shape of 2D array/ motif: diam, pore size	Distance between motifs (pitch)	Average height of 2D array	Field of application	Ref
Recrystallisation of S and T layer							
2D array	Recrystallisation of T-layer	500 nm x 500 nm	Cylindrical: pore 6.5 nm	13 nm	ND	ND	1
2D array	Ca2+ coordination of monomers from S-layer	2 µm x 10 µm	Square	13 nm	1-2 layers (9-15 nm)	ND	2
2D array	Recrystallization of S-layer fused to streptavidin	ND	Square: ND	10	1 layer (4.5 nm)	Nanopatterned matrix to arrange biotinylated compounds on a surface	3
Disulfide formation or metal coordination							
Nanorod, 2D array	Metal coordination of tunable acetyltransferase modified by bipyridine-alanine	2 µm x 2 µm	Honeycomb: pore 5 nm*	10 nm	1 layer (7 nm)	Tunable multicomponent assemblies	4
Nanotube, 2D to 3D	different Zn2+ coordination of modified monomers	15 µm x 15 µm	Rectangular: pore 3 nm*	ND	1 layer (ND) to few layers (2D stacking)	ND	5
2D array	Disulfide formation or metal coordination of modified TMVCP[a]	1 µm x 1 µm	Square, honeycomb: pore 8 nm*	19-21 nm	2-3 layers (20-30 nm[a])	Nanotechnology**	6
2D array	Disulfide formation or metal coordination of modified RhuA[a]	2 µm x 2 µm	Square: pore 1-4 nm	9-11 nm	1 layer (5 nm*) to few layers	ND	7
2D array	Metal coordination of modified STM4215	100 µm	Honeycomb: pore 5 nm	7 nm	1 layer (5 nm)	Nanotechnology**	8
2D array	Disulfide formation of modified rHuHF (ferritin)	ND	Square: pore 8 nm*	12.5 nm	ND	Proof of concept for further application to other proteins	9
2D array	Disulfide formation modified RhuA[a]	2.4 µm x 2.4 µm	Square: pore 6 nm*	11.4 nm	ND	Creation of AuNP lattices for nanotechnology	10
Lectin/Sugar and Rodhamin dimerization							
Nanorod, and ribbon, 2D array, 3D	Tetrameric lectin (LECA) connected by sugar and rhodamin interaction	100 nm x 100 nm	Square: pore 3 nm*	5 nm	1 layer (2 nm) to few layers (2D stacking)	Tunable multicomponent assemblies	11
2D array	Tetrameric lectin (CONA) connected by sugar and rhodamin interaction	100 µm x100 µm	Square: pore 7 nm*	8 nm*	Several layers (200 nm)	Tunable multicomponent assemblies	12
Genetic fusion of subunits from protein assemblies fusion							
2D array	Interaction between receptor (streptavidin) and ligand (Steptag)-fused protein	ND	Square: pore 8 nm*	14 nm	1 layer (ND)	Design biomaterials with diverse properties	13
Hydrophobic interaction							
2D array	Non-covalent interaction of class1-2 hydrophobins	1 µm x 1 µm*	-Rodlet (class 1): no pores -Mesh (class 2): pore 20-30 nm	ND	-Rodlet ND -Mesh, 1 layer (2 nm)	Modification of the wettability of hydrophobic surface	14
2D array,3D	Hydrophobic interaction between amyloid residues of modified ferritin	500 nm x 500 nm*	Square: cage 8 nm*	12.6 nm	1 layer (10 nm) to several layers (114 nm)	Control 2D or 3D protein self-assemblies	15
2D array, 3D	Hydrophobic interaction between aromatic amino acids modified ferritin	ND	Square: cage 8 nm	11.4 nm	1 layer (11.5 nm) to several layers (ND)	Templates for the fabrication of 2D, 3D nanoparticle arrays	16
De novo computational design							
2D array	Computational design of protein/protein interaction	1 µm x 1 µm	Ring, rectangular or triangular: pore < 5 nm	5 - 15 nm	1 layer, 3-8 nm	Nanotechnology**	17
2D array	Computational design of protein/protein interaction	200 nm x 200 nm	Rectangular: pore 2.3 nm*	4 nm*	1 layer (2.4 nm)	Programmable protein assembly	18
Nanowire,2D array	Computational design of protein-surface interaction	ND ou 850 mm x 850 mm*	Tunable honeycomb: pore (9-30 nm)	Tunable distance (11-30 nm)	1 layer (ND)	Design of protein–inorganic hybrid materials	19
Enzyme-triggered covalent protein assembly							
Nanotube, 2D array	Covalent assembly of modified SP1 via enzyme catalysis	200 nm x 200 nm	Honeycomb: pore 2.5 nm	11 nm*	1 layer (4 nm)	Energy transfer through quantum-dot	20
Head-tail interaction							
3D array	Oligomerization domain	2 µm x 2 µm	Honeycomb: pore 5 nm	8 nm	Helicoidal self-assembly (31 nm = 40 layers)	Pores modification for Nanotechnology	This work

*Values deduced from publication, ** Potential applications, no work done to test feasibility. ND, not described.

Table S2. Amino acid sequences of the N- and C-terminal extensions of the different proteins used.

	N-terminal extension	C-terminal extension
GbLFY-SAM	MKHHHHHHPMSDYDIPTTENLYFQGA	KKLDLFVDVDGKRKADENALDTLSQA
GbLFY-SAM N-terminal mutant	MKHHHHHHP	KKLDLFVDVDGKRKADENALDTLSQA
GbLFY-SAM shortest N-terminal mutant	MHHHHHH	KKLDLFVDVDGKRKADENALDTLSQA
GbLFY-SAM short C-terminal mutant	MKHHHHHHPMSDYDIPTTENLYFQGA	KKLDA
GbLFY-SAM K110C C-terminal mutant	MKHHHHHHPMSDYDIPTTENLYFQGA	CKLDLFVDVDGKRKADENALDTLSQA
GbLFY-SAM linker 3CH C-terminal mutant	MKHHHHHHPMSDYDIPTTENLYFQGA	GGSGGSCHCHCHC

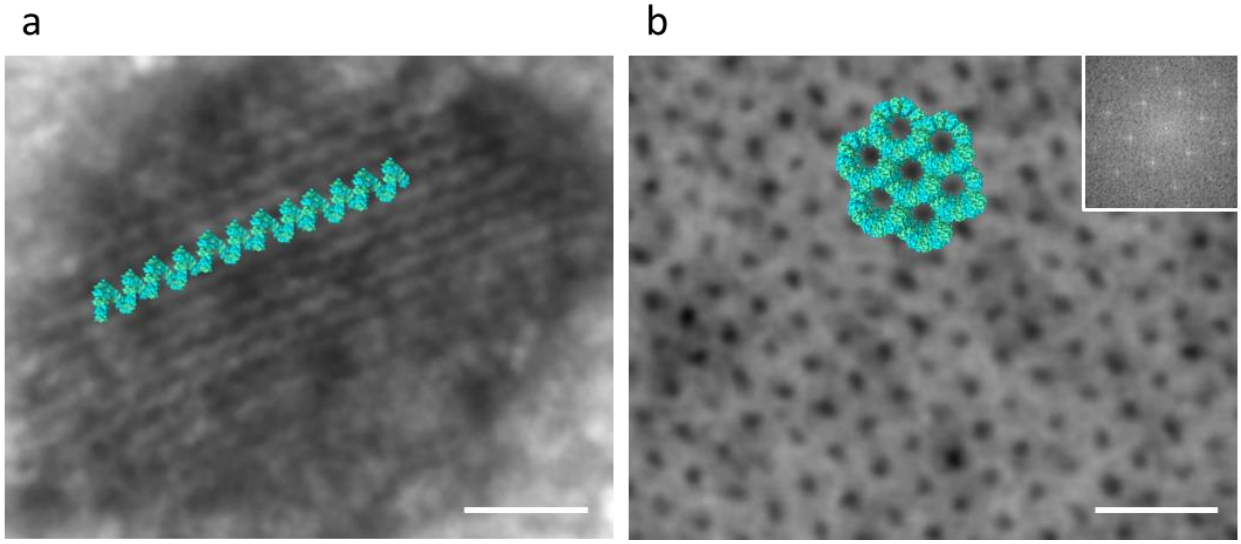

Figure S1. Superposition of GbLFY-SAM crystallographic structures to the self-assemblies. (a) Superposition of one helix to the self-assembly of GbLFY-SAM without its N-terminal. (b) Superposition of the honeycomb to the self-assembly of GbLFY-SAM with its N-terminal extension. The scale bars are 30 nm in both images.

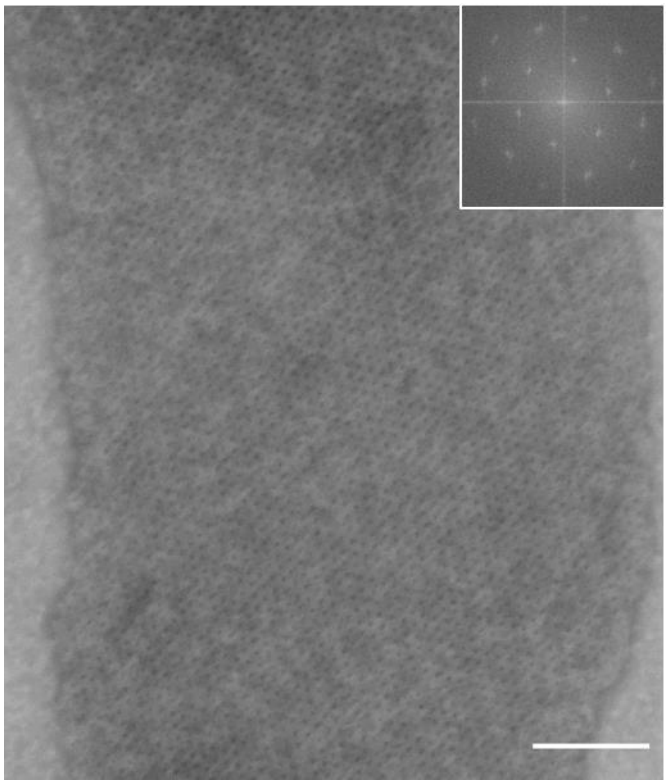

Figure S2. STEM image of GbLFY-SAM self-assembling in a honeycomb structure despite the addition of 1 mM EDTA. The Fourier Transform shown in inset confirm the conservation of the lattice parameters. Scale bar: 100 nm.

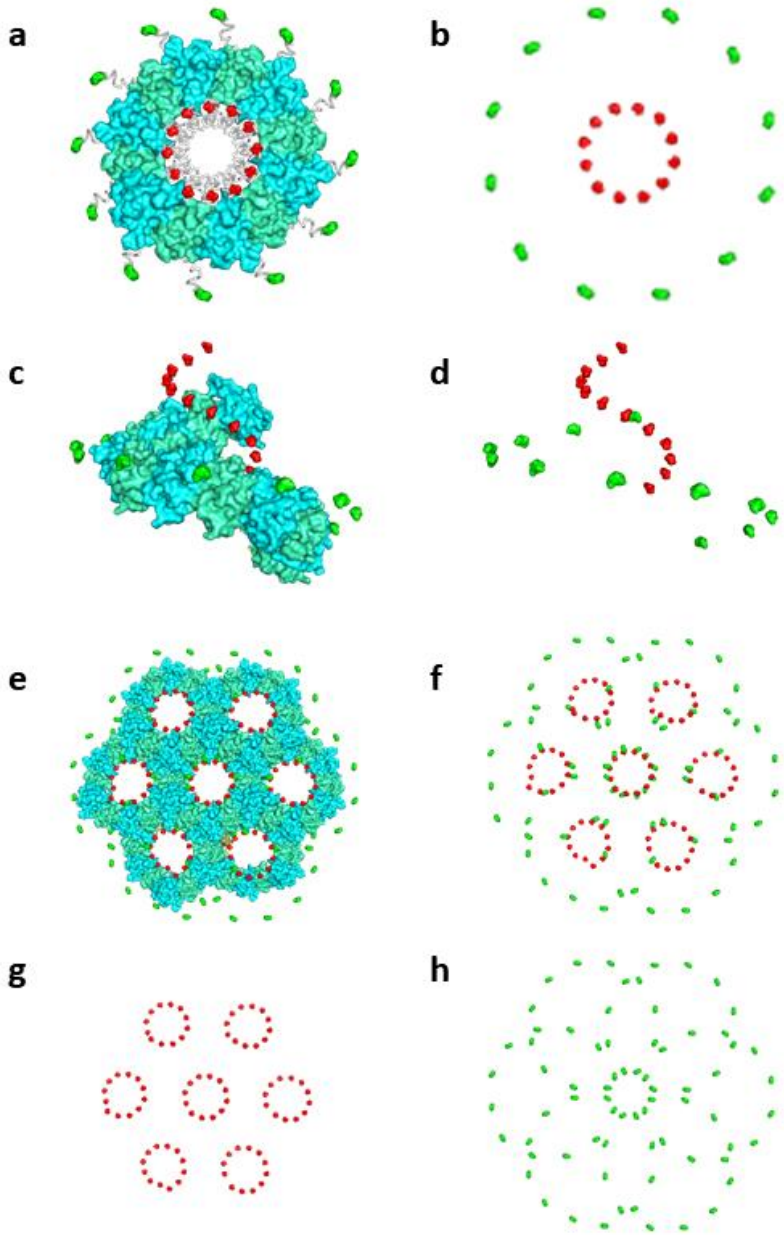

Figure S3. The polymeric honeycomb structure has a modular platform for broad applications. (a) view of 12 monomers modelled by I-TASSER forming one helix round with the first residues of the N-terminal shown as green surface and the last residues shown as red surface. For better visibility, only 12 out of 40 monomers are represented. (b) same representation with only the first and last residues shown as green and red surfaces. (c) and (d) lateral view of one helical polymer. (e) honeycomb formation by interaction between one central helical polymer and 6 helical polymers. (f) same representation with only the first and last residues shown as green and red surfaces (g) only the last residues shown as red surfaces or (h) only the first residues shown as green surfaces. Both N- and C-terminal extension are located inside the pores and could be used for specific grafting.

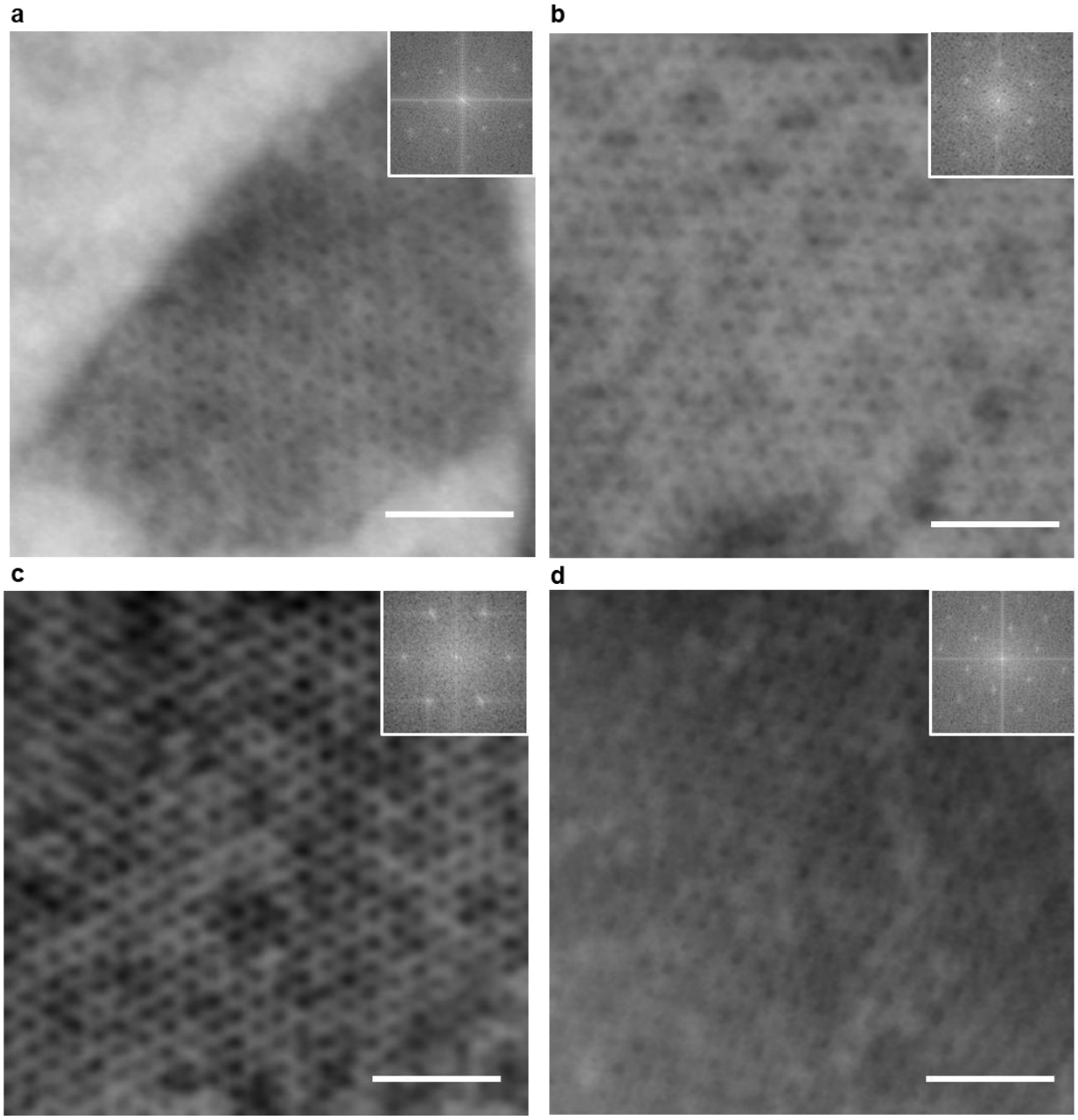

Figure S4. STEM image of engineered N-terminal (a) and C-terminal (b-d) GbLFY-SAM extension. (a) Self-assembly with only the first seven amino acid residues of the N-terminal extension. (b) Self-assembly with a deletion of the C-terminal part. (c) Self-assembly of GbLFY-SAM K110C. (d) Self-assembly with a GGSGGSCHCHC sequence instead of the C-terminal extension. The Fourier transform images shown in insert indicate that the engineered GbLFY-SAM have an architecture and dimensions similar to those observed with GbLFY-SAM. The scale bars are 50 nm in all the images.

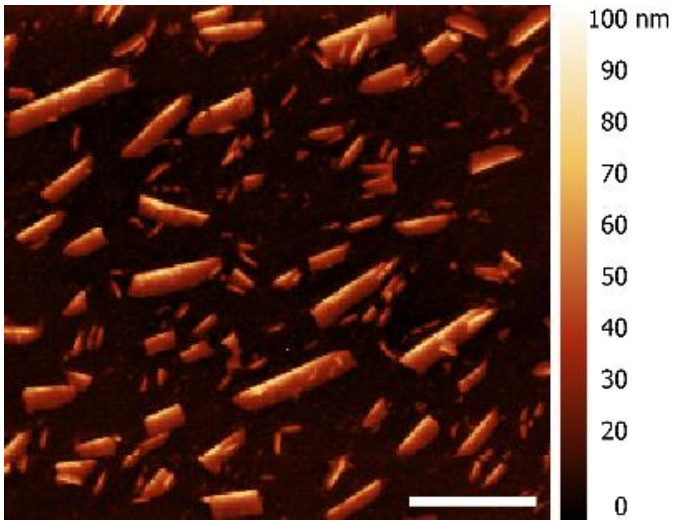

Figure S5. Measurement of the average height of the honeycomb of GbLFY-SAM with its N-terminal extension using AFM on several individual crystals. Scale bar: 1 µm.

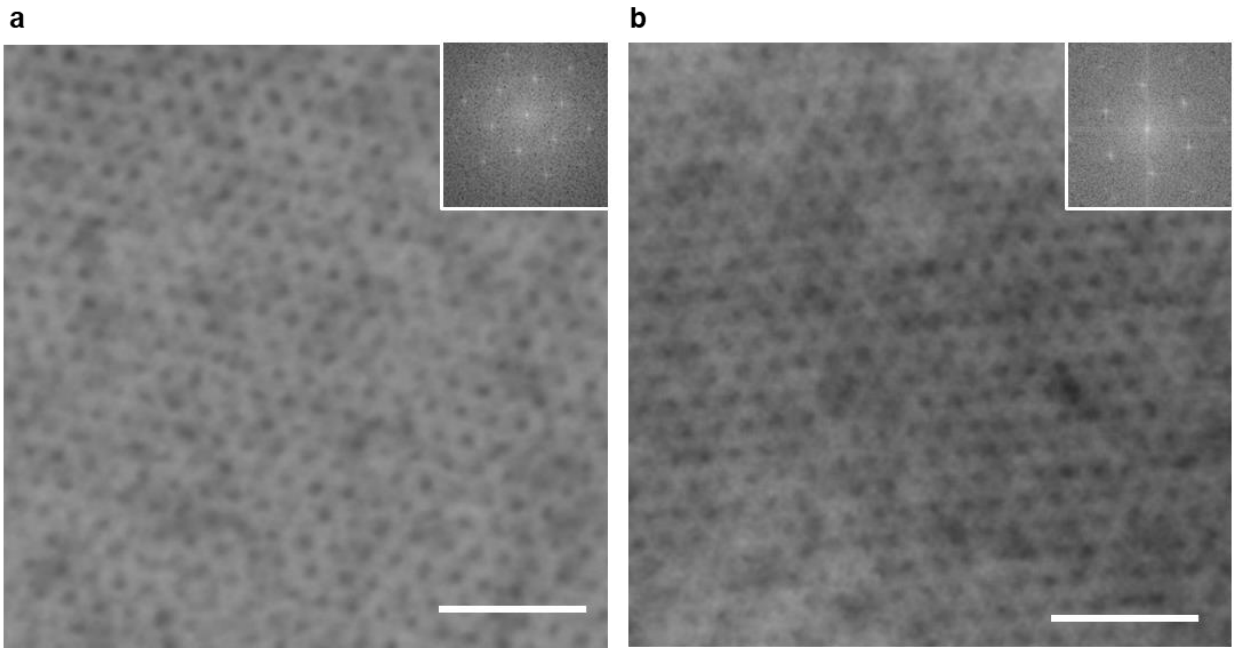

Figure. S6. STEM image of GbLFY-SAM self-assembly on hydrophobic (a) and hydrophilic (b) silicon nitride. (a) Self-assembly on a hydrophobic silicon nitride coated with alumina and fluoro-methyl-silane. (b) Self-assembly on a hydrophilic silicon nitride coated with hydroxylated alumina. The fast Fourier transform of the images shown in insert indicate that the self-assemblies have an architecture and dimensions similar to those observed onto carbon and silicon surfaces. The scale bars are 50 nm in both images.

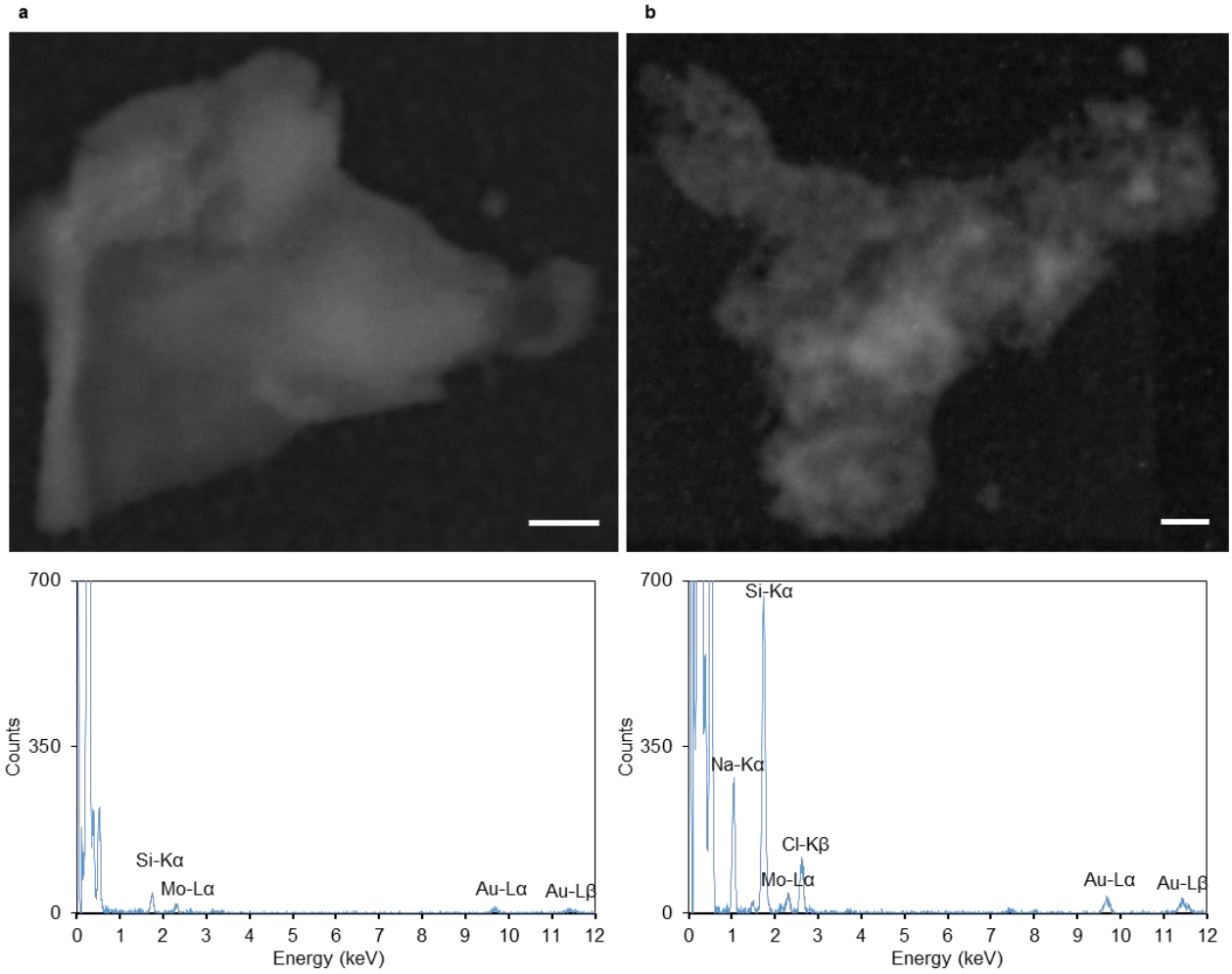

Figure S7. In presence of 1 mM EDTA, Ni^{2+} salt are desorbed from GbLFY-SAM self-assembly. (a) *Top,* STEM image in dark field mode of an unstained self-assembly. *Bottom,* EDX spectrum of the self-assembly showing the absence of uranyl acetate. (b) *Top,* STEM image in dark field mode of a self-assembly after the Ni^{2+} salt desorption chelated thanks to the 1 mM EDTA. *Bottom,* EDX spectrum of the self-assembly showing that nickel is out of the self-assembly. All the scale bars are 100 nm in both images.

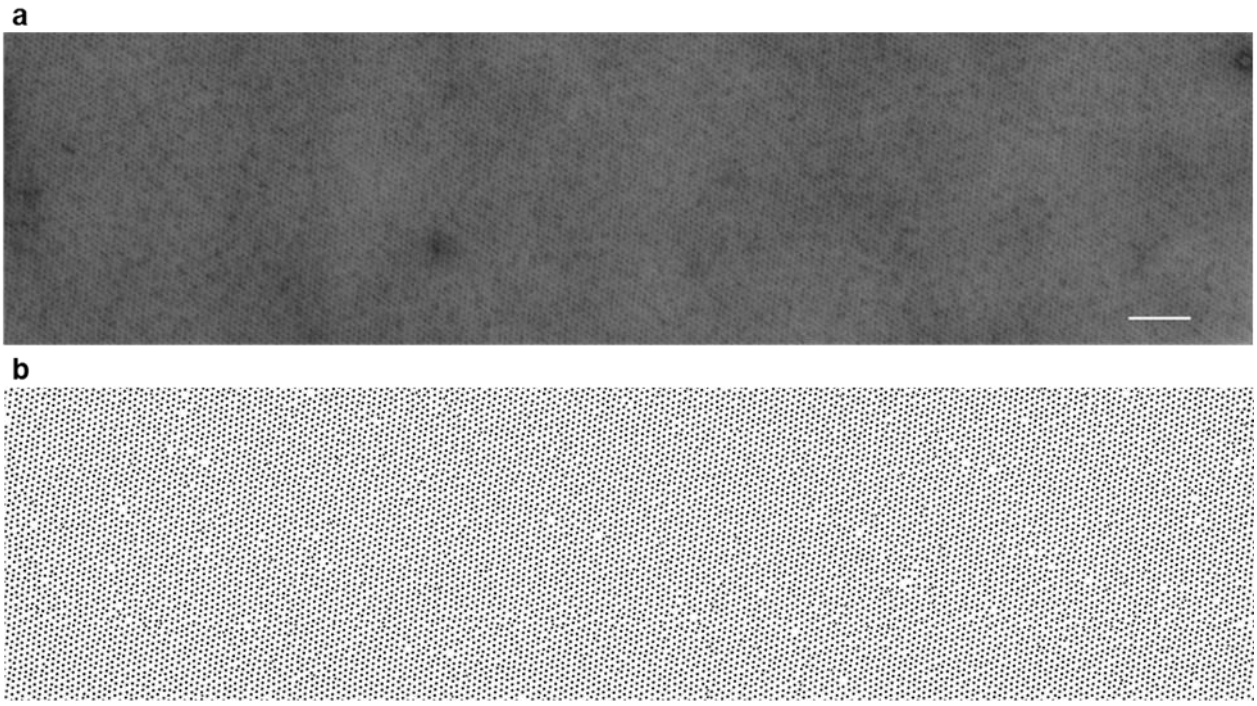

Figure S8. Self-assembly as a platform for specific grafting of a huge number of ligands. (a) Self-assembly of GbLFY-SAM on a 1 μm^2 carbon surface. Scale bar: 100 nm. (b) Determination of the number of honeycomb pores on the surface of 1 μm^2 shown in (a) using Fiji. In this area the self-assembly provides a surface density of 11 835 available pores per μm^2. Considering that each pore corresponds to a stacking of an average of 40 GbLFY-SAM monomers, and assuming that at least one terminal extension of each monomer could be modified for grafting, this self-assembly presents 485 235/μm^2 specific grafting sites for metal, organic or inorganic compounds for various applications.

(1) Aebi, U.; Smith, P. R.; Dubochet, J.; Henry, C.; Kellenberger, E. A Study of the Structure of the T-Layer of Bacillus Brevis. *J. Supramol. Struct.* **1973**, *1* (6), 498–522. https://doi.org/10.1002/jss.400010606.
(2) Györvary, E. S.; Stein, O.; Pum, D.; Sleytr, U. B. Self-Assembly and Recrystallization of Bacterial S-Layer Proteins at Silicon Supports Imaged in Real Time by Atomic Force Microscopy. *J. Microsc.* **2003**, *212* (3), 300–306.
(3) Moll, D.; Huber, C.; Schlegel, B.; Pum, D.; Sleytr, U. B.; Sara, M. S-Layer-Streptavidin Fusion Proteins as Template for Nanopatterned Molecular Arrays. *Proc. Natl. Acad. Sci.* **2002**, *99* (23), 14646–14651. https://doi.org/10.1073/pnas.232299399.
(4) Yang, M.; Song, W. J. Diverse Protein Assembly Driven by Metal and Chelating Amino Acids with Selectivity and Tunability. *Nat. Commun.* **2019**, *10* (1). https://doi.org/10.1038/s41467-019-13491-w.
(5) Brodin, J. D.; Ambroggio, X. I.; Tang, C.; Parent, K. N.; Baker, T. S.; Tezcan, F. A. Metal-Directed, Chemically Tunable Assembly of One-, Two- and Three-Dimensional Crystalline Protein Arrays. *Nat. Chem.* **2012**, *4* (5), 375–382. https://doi.org/10.1038/nchem.1290.
(6) Zhang, J.; Wang, X.; Zhou, K.; Chen, G.; Wang, Q. Self-Assembly of Protein Crystals with Different Crystal Structures Using Tobacco Mosaic Virus Coat Protein as a Building Block. *ACS Nano* **2018**, *12* (2), 1673–1679. https://doi.org/10.1021/acsnano.7b08316.
(7) Suzuki, Y.; Cardone, G.; Restrepo, D.; Zavattieri, P. D.; Baker, T. S.; Tezcan, F. A. Self-Assembly of Coherently Dynamic, Auxetic, Two-Dimensional Protein Crystals. *Nature* **2016**, *533* (7603), 369–373. https://doi.org/10.1038/nature17633.
(8) Matthaei, J. F.; DiMaio, F.; Richards, J. J.; Pozzo, L. D.; Baker, D.; Baneyx, F. Designing Two-Dimensional Protein Arrays through Fusion of Multimers and Interface Mutations. *Nano Lett.* **2015**, *15* (8), 5235–5239. https://doi.org/10.1021/acs.nanolett.5b01499.
(9) Zhou, K.; Chen, H.; Zhang, S.; Wang, Y.; Zhao, G. Disulfide-Mediated Reversible Two-Dimensional Self-Assembly of Protein Nanocages. *Chem. Commun.* **2019**, *55* (52), 7510–7513. https://doi.org/10.1039/C9CC03085A.
(10) Du, M.; Zhou, K.; Wang, X.; Zhang, J.; Zhang, Y.; Dong, J.; Wu, L.; Qiao, Z.; Chen, G.; Wang, Q. Precise Fabrication of De Novo Nanoparticle Lattices on Dynamic 2D Protein Crystalline Lattices. *Nano Lett.* **2020**, *20* (2), 1154–1160. https://doi.org/10.1021/acs.nanolett.9b04574.
(11) Yang, G.; Ding, H.; Kochovski, Z.; Hu, R.; Lu, Y.; Ma, Y.; Chen, G.; Jiang, M. Highly Ordered Self-Assembly of Native Proteins into 1D, 2D, and 3D Structures Modulated by the Tether Length of Assembly-Inducing Ligands.

Angew. Chem. Int. Ed. **2017**, *56* (36), 10691–10695. https://doi.org/10.1002/anie.201703052.
(12) Sakai, F.; Yang, G.; Weiss, M. S.; Liu, Y.; Chen, G.; Jiang, M. Protein Crystalline Frameworks with Controllable Interpenetration Directed by Dual Supramolecular Interactions. *Nat. Commun.* **2014**, *5* (1). https://doi.org/10.1038/ncomms5634.
(13) Sinclair, J. C.; Davies, K. M.; Vénien-Bryan, C.; Noble, M. E. M. Generation of Protein Lattices by Fusing Proteins with Matching Rotational Symmetry. *Nat. Nanotechnol.* **2011**, *6* (9), 558–562. https://doi.org/10.1038/nnano.2011.122.
(14) Lo, V.; Ren, Q.; Pham, C.; Morris, V.; Kwan, A.; Sunde, M. Fungal Hydrophobin Proteins Produce Self-Assembling Protein Films with Diverse Structure and Chemical Stability. *Nanomaterials* **2014**, *4* (3), 827–843. https://doi.org/10.3390/nano4030827.
(15) Zheng, B.; Zhou, K.; Zhang, T.; Lv, C.; Zhao, G. Designed Two- and Three-Dimensional Protein Nanocage Networks Driven by Hydrophobic Interactions Contributed by Amyloidogenic Motifs. *Nano Lett.* **2019**, *19* (6), 4023–4028. https://doi.org/10.1021/acs.nanolett.9b01365.
(16) Zhou, K.; Zang, J.; Chen, H.; Wang, W.; Wang, H.; Zhao, G. On-Axis Alignment of Protein Nanocage Assemblies from 2D to 3D through the Aromatic Stacking Interactions of Amino Acid Residues. *ACS Nano* **2018**, *12* (11), 11323–11332. https://doi.org/10.1021/acsnano.8b06091.
(17) Gonen, S.; DiMaio, F.; Gonen, T.; Baker, D. Design of Ordered Two-Dimensional Arrays Mediated by Noncovalent Protein-Protein Interfaces. *Science* **2015**, *348* (6241), 1365–1368. https://doi.org/10.1126/science.aaa9897.
(18) Chen, Z.; Johnson, M. C.; Chen, J.; Bick, M. J.; Boyken, S. E.; Lin, B.; De Yoreo, J. J.; Kollman, J. M.; Baker, D.; DiMaio, F. Self-Assembling 2D Arrays with *de Novo* Protein Building Blocks. *J. Am. Chem. Soc.* **2019**, *141* (22), 8891–8895. https://doi.org/10.1021/jacs.9b01978.
(19) Pyles, H.; Zhang, S.; De Yoreo, J. J.; Baker, D. Controlling Protein Assembly on Inorganic Crystals through Designed Protein Interfaces. *Nature* **2019**, *571* (7764), 251–256. https://doi.org/10.1038/s41586-019-1361-6.
(20) Zhao, L.; Zou, H.; Zhang, H.; Sun, H.; Wang, T.; Pan, T.; Li, X.; Bai, Y.; Qiao, S.; Luo, Q.; Xu, J.; Hou, C.; Liu, J. Enzyme-Triggered Defined Protein Nanoarrays: Efficient Light-Harvesting Systems to Mimic Chloroplasts. *ACS Nano* **2017**, *11* (1), 938–945. https://doi.org/10.1021/acsnano.6b07527.